Received: 31 March 2020 | Revised: 20 April 2020 | Accepted: 21 April 2020

DOI: 10.1002/aoc.5795

FULL PAPER

Applied Organometallic Chemistry WILEY

Photocatalytic Cr(VI) sequestration and photo-Fenton bisphenol A decomposition over white light responsive PANI/MIL-88A(Fe)

Dan-Dan Chen | Xiao-Hong Yi | Li Ling | Chong-Chen Wang | Peng Wang

Beijing Key Laboratory of Functional Materials for Building Structure and Environment Remediation, Beijing University of Civil Engineering and Architecture, Beijing, 100044, China

Correspondence
Chong-Chen Wang, Beijing Key Laboratory of Functional Materials for Building Structure and Environment Remediation, Beijing University of Civil Engineering and Architecture, Beijing, 100044, China.
Email: wangchongchen@bucea.edu.cn; chongchenwang@126.com

Funding information
Beijing Talent Project, Grant/Award Number: 2019A22; BUCEA Post Graduate Innovation Project, Grant/Award Number: PG2019041; Great Wall Scholars Training Program Project of Beijing Municipality Universities, Grant/Award Number: CIT and TCD20180323; National Natural Science Foundation of China, Grant/Award Numbers: 51578034, 51878023

Polyaniline (PANI)/MIL-88A(Fe) (Px@M88) composites were constructed through a simple one-pot hydrothermal method. The photocatalytic and photo-Fenton activities of Px@M88 composites toward reduction of Cr(VI) and degradation organic pollutants were explored by white light irradiation. PANI, as a conductive polymer, can improve MIL-88A(Fe)'s conductivity and the efficiency of photogenerated e^-–h^+ pair separation. In the presence of H_2O_2, a photo-Fenton reaction occured to boost the degradation efficiency of organic pollutants like bisphenol A. In addition, P9@M88 showed excellent recycling and stability in cycling experiments. Finally, a possible reaction mechanism for photocatalytic degradation was proposed and verified by X-ray photoelectron spectroscopy and electron spin resonance determination and electrochemical characterizations.

KEYWORDS
bisphenol A, Cr(VI) reduction, MIL-88A(Fe), photocatalyst, polyaniline

1 | INTRODUCTION

In recent years, metal–organic frameworks (MOFs) as potential photocatalysts have been extensively used in CO_2 capture and reduction,[1–3] H_2 evolution,[4,5] organic pollutant degradation[6–8] and Cr(VI) reduction,[9,10] owing to their merits of high porosity, high specific surface area, adjustable pore size, easy modification structure and diversified functions.[11–14] Most MOFs show good photocatalytic properties only under ultraviolet light illumination, which limits their potential applications under visible light or sunlight. Fe-based MOFs including but not limited to MIL-88(Fe), MIL-100 (Fe) and MIL-101(Fe) can be excited by light with wavelength >420 nm.[15,16] However, they still suffer from some bottleneck problems like inadequate stability, fast photogenerated electron–hole recombination and poor conductivity. In order to further solve the above-stated problems of Fe-MOFs, a strategy to combine semiconductor materials (TiO_2, g-C_3N_4),[15,17,18] metal nanoparticles[14,19] and conductive polymers[20] is often adopted. He et al. constructed MIL-101(Fe)/TiO_2 composite to enhance photocatalytic efficiency toward tetracycline decomposition by tsunlight irradiation.[21] Chen et al. investigated whether MIL-100(Fe)/PANI (polyaniline) composites can promote the photocatalytic activity of tetracycline decomposition and Cr(VI) sequestration under white light illumination.[22]

 © 2020 John Wiley & Sons, Ltd.

Hexavalent chromium Cr(VI), in the form of $Cr_2O_7^{2-}$, is a common highly toxic pollutant in the water environment, and excessive Cr(VI) (over 10 mg/L) might lead to a lethal effect on aquatic life. Photocatalysis is an effective strategy to reduce highly toxic Cr(VI) into less toxic Cr(III).[9,23] In addition, there are also large numbers of organic pollutants like organic dyes and pharmaceutical and personal care products in sewage,[24–26] which pose a serious threat to the ecological environment and human health.

Inspired by our previous preparation of Z-scheme MIL-100(Fe)/PANI[22] and high-throughput yields of MIL-88A(Fe),[27] in this study, PANI was selected to modify MIL-88A(Fe) for construction of PANI/MIL-88A (Fe) (Px@M88) composites. PANI is a good conductive polymer with π–π conjugation, which can facilitate interfacial electron migration and accelerate photogenerated electron–hole separation. In addition, PANI exhibits good light utilization within the visible light region (>420 nm), which can improve the use of visible light and boost the photocatalytic activity.[28] The introduction of PANI to combine MIL-88A(Fe) for constructing PANI/MIL-88A (Fe) (Px@M88) might accomplish improved photogenerated carrier separation and enhanced conductivity. Therefore, the photocatalytic activities and efficiencies of pollutant elimination are enhanced.

2 | MATERIALS AND METHODS

All reagents except for PANI were obtained commercially from J&K and used directly. PANI with molecular weight 50,000–60,000 and electric conductivity 2 s/cm was purchased from Taizhou Yongjia Trade Co. Ltd.

A one-pot hydrothermal method was used to synthesize the PANI/MIL-88A(Fe) composite materials by adjusting the mass ratio of MIL-88A(Fe) vs. PANI. A certain amount of PANI powder was dispersed in 20 mL N, N-dimethylformamide (DMF). Then, 1.352 g $FeCl_3{\cdot}6H_2O$ and 0.580 g fumaric acid ($C_4H_4O_4$) were added to 30 ml DMF and the mixture was stirred vigorously. The PANI solution was dropped into the above mixture solution slowly and stirred vigorously for 60 min. The homogeneous mixture of PANI, $FeCl_3{\cdot}6H_2O$ and fumaric acid was put into a Teflon-lined autoclave (75.0 ml) to react hydrothermally at 100°C for 12 h. After cooling down to the ambient temperature, the products were obtained from the solution via centrifugation and washed three times with DMF, ethanol and water, respectively. The harvested powder was dried at 60°C in the thermostatic vacuum drier, and labeled as Px@M88 (Px is the percentage of the initial input mass ratio of PANI/$FeCl_3{\cdot}6H_2O$, in which x equals 1, 4, 7, 9 and 10, respectively). As a comparison, pure MIL-88A(Fe) was also produced under the same reaction conditions as PANI/MIL-88A (Fe) composites except for there being no addition of PANI.[8]

3 | RESULTS AND DISCUSSION

From the results of powder X-ray diffraction (PXRD) patterns (Figure 1a), the sharp and intense diffraction peaks at $2\theta = 11.59°$ and $2\theta = 17–25°$ revealed that the structure of MIL-88A(Fe) is well preserved in Px@M88, implying that the combination of PANI and MIL-88A(Fe) has no noticeable influence on the structure of MIL-88A(Fe). In Px@M88's PXRD patterns, the diffraction peak of PANI was not observed, owing to both the low content and the amorphous phase of PANI.[22] As showed in Figure 1b, all of the scanning electron microscopy (SEM) and transmission electron microscopy images of P9@M88 revealed that the tiny PANI particles were distributed over the well-crystallized MIL-88A(Fe) with a spindle shape.[29,30] The elemental mapping of P9@M88 (Figure 1a and Figure S1) obtained from SEM verified that Fe and O elements in MIL-88A(Fe) and N element in PANI were detected. The Fe, O and N elements were evenly distributed over P9@M88, further indicating the successful composite between MIL-88A(Fe) and PANI.

The formation of P9@M88 was further affirmed by X-ray photoelectron spectroscopy (XPS) determination and the elements of C, O, N, and Fe were detected in the photocatalysts (Figure S3). The C 1 s, O 1 s, N 1 s and Fe 2p spectra of P9@M88 are described in detail in the Supplementary Information, in which the typical peaks of Fe elements in MIL-88A(Fe) and protonated amine units (-NH_2^+-) of PANI are presented simultaneously in the spectra of P9@M88.

The UV-vis diffuse reflectance spectrum (DRS) is commonly used to elucidate the optical activities of photocatalyst materials.[31] Figure 1c showed that the light absorption intensities of Px@M88 are higher than that of the original MIL-88A(Fe) in the range of 420–800 nm, in which P9@M88 exhibits the highest visible light absorption intensity. The band gap (Eg) of P9@M88 was calculated as 2.65 eV using the Beer–Lambert equation (Equation 1), lower than that of pristine MIL-88A(Fe) (2.75 eV). The band-edge of optical absorption of P9@M88 was estimated as ca. 468 nm, implying that it can utilize more solar energy to generate light-induced charge carriers for boosted photocatalytic performance.[32]

$$(ahv)^2 = A\,(hv - Eg) \tag{1}$$

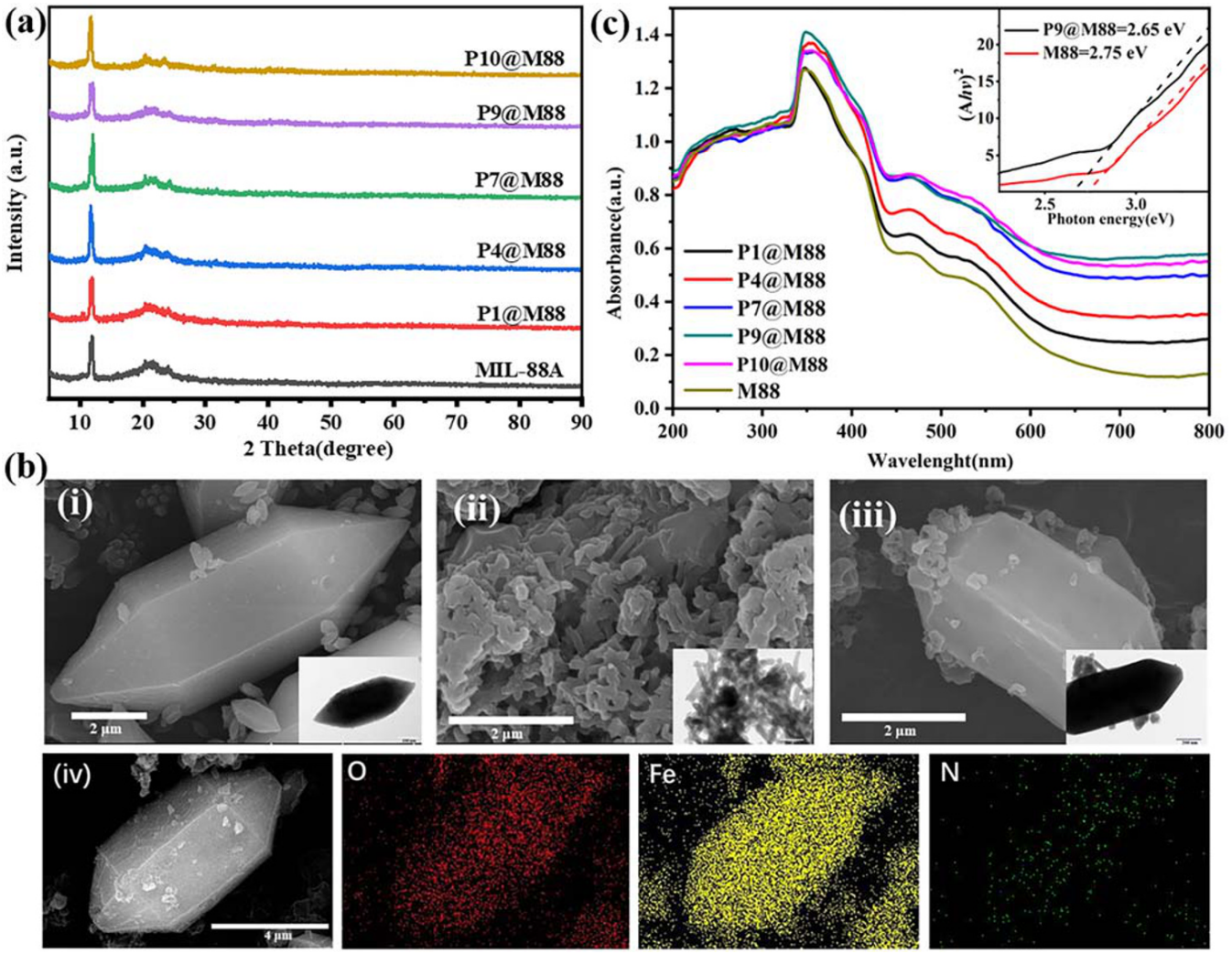

FIGURE 1 (a) XRD patterns of MIL-88A, PANI and Px@M88 photocatalysts; (b) scanning electron microscopy images of (i) MIL-88A, (ii) PANI, (iii) P9@M88 particles, the insets showing the corresponding transmission electron microscopy images and (iv) the elemental mapping of P9@M88; (c) UV–vis diffuse reflectance spectra of MIL-88A and Px@M88 photocatalysts and the insets are corresponding Tauc plots

where α, $h\nu$ and A are the diffuse absorption coefficient, the photonic energy and the constant, respectively.

In order to screen out the optimum catalyst, the photocatalytic Cr(VI) reduction efficiencies of different types of Px@M88 were studied (Figure 2a). It could be seen that the Cr(VI) photoreduction efficiencies of Px@M88 composite were higher than those of MIL-88A (Fe) (Figure 2b). The optimal P9@M88 demonstrated the best photocatalytic efficiency and biggest reaction rate, in which the Cr(VI) was completely removed within 50 min. The P9@M88 composite could accomplish 40% Cr(VI) removal via adsorption in dark conditions. Under the irradiation of white light, the absorbed Cr(VI) was gradually reduced to Cr(III) by P9@M88 photocatalyst. Eventually, the total Cr(VI) in the solution was completely converted to Cr(III). The change in total chromium in the solution is illustrated in Figure S4.

Therefore, P9@M88 was selected as the best catalyst to investigate the influence of pH, low-weight organic acids as hole scavengers and foreign inorganic ions on Cr(VI). It was seen that P9@M88 exhibited the best photocatalytic efficiency of Cr(VI) reduction at pH 2 (Figure S5a), owing to the plentiful H^+ further promoting the conversion of Cr(VI) to Cr(III) (Equation 2).[33]

$$Cr_2O_7^{2-} + 14H^+ + 6e^- \rightarrow 2Cr^{3+} + 7H_2O \qquad (2)$$

Some small-weight organic acids like tartaric acid, oxalic acid and citric acid are often used as h^+ scavengers to capture the photogenerated holes and to accelerate charge carrier separation for improving the efficiency of Cr(VI) reduction (Figure S5b). The results demonstrated that the addition of small-weight organic acid chemicals can boost the Cr(VI) reduction efficiency.

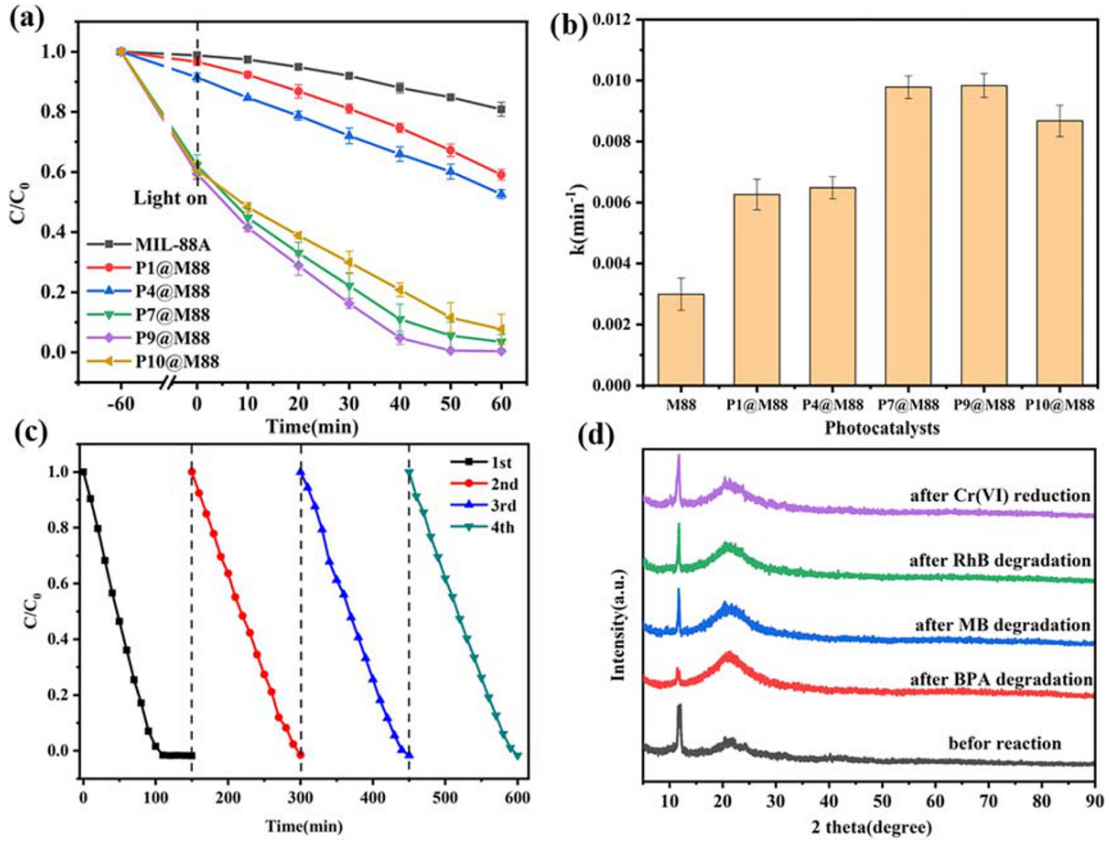

FIGURE 2 (a) Photocatalytic activities in Cr(VI) reduction over different samples under white light irradiation; (b) the photocatalytic reduction rates (*k* values) of samples prepared toward Cr(VI); (c) cycle experiments with P9@M88 for Cr(VI) reduction under white light; and (d) powder X-ray diffraction (PXRD) patterns of P9@M88 before and after the circular reaction

Additionally, the effects of co-existing ions and practical water application were investigated. Tap water and lake water were employed to configure the simulated wastewater containing Cr(VI) solution. The results demonstrated that the reduction efficiency of Cr(VI) was slightly suppressed in simulated sewage configured with tap water and lake water (Figure S5c). It is believed that some cations like Na^+, K^+, Ca^{2+} and Mg^{2+} will not exert significant impacts on the photocatalytic process, because these cations with high stability and oxidation state cannot react with the photogenerated electrons or holes.[34] Our previous Box-Behnken experiments demonstrated that the anions like Cl^-, and SO_4^{2-} along with dissolved organic matter (DOM) in the simulated solution containing Cr(VI) will impact Cr(VI) reduction efficiency subject to their concentrations.[35] Also, considering that the P9@M88's surface was positively charged at pH 2, these co-existing anions might compete with $Cr_2O_7^{2-}$ to occupy the adsorptive sites through electrostatic attraction, leading to reduced photoreduction efficiency.

The recyclability and stability of the P9@M88 composites have been verified by cyclic experiments (Figure 2c), in which the Cr(VI) reduction efficiency can be maintained at 99% after the fourth run's operation. In this study, the Fe ions being leached out to the solution after the four cyclic experiments were measured as 0.15 ± 0.05 mg/L by inductively coupled plasma–mass spectrometry. The XRD patterns of P9@M88 after four runs were completely consistent with the original MIL-88A(Fe) samples (the purple line in Figure 2d). The stability of the P9@M88 was further affirmed from the SEM images as illustrated in Figure 3d, in which the spindle shape of MIL-88A(Fe) was perfectly maintained.

Considering that the iron element in MIL-88A (Fe) can undergo a Fenton reaction in the presence of H_2O_2 to improve the degradation rate of organic pollutants,[36,37] some organic pollutants like BPA (bisphenol A), MB (methylene blue) and RhB (Rhodamine B) were selected to test the photo-Fenton degradation activity of P9@M88.

As displayed in Figure 3a, no BPA removal was observed under irradiation with white light for 60 min in the presence of PANI. Meanwhile, about 99% BPA was degraded by MIL-88A(Fe), which could be realized by white light irradiation for 60 min. As for Px@M88 composites, the BPA degradation efficiencies increased gradually with the increase in PANI contents. However, with the excessive increase of PANI content, e.g. 10%, the BPA

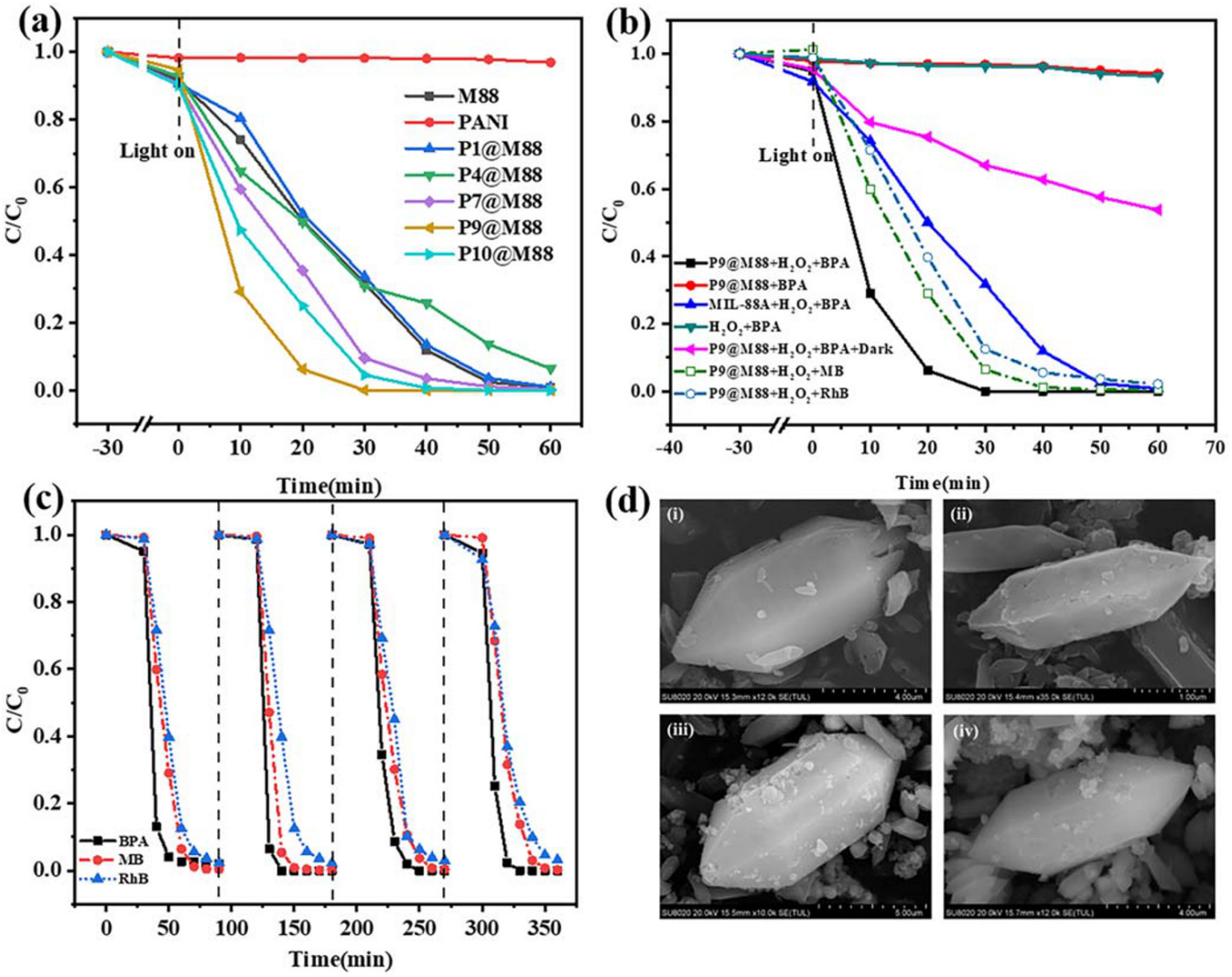

FIGURE 3 (a) Photocatalytic degradation of BPA over different samples under white light irradiation; (b) photocatalytic degradation of BPA, MB and RhB under different conditions; (c) reusability of P9@M88 for the photocatalytic degradation of organic pollutants; and (d) SEM images of P9@M88 before and after the circular reaction. Reaction conditions: 200 mg/L of photocatalyst, 50 ml of 10 mg/L organic pollutants, 0.4 ml/L of H_2O_2

removal efficiency decreased. As a result, 100% BPA degradation could be achieved over P9@M88 within 30 min; however the pristine MIL-88A(Fe) could only accomplish 63% BPA degradation with 30 min. Figure 3b presents the photo-Fenton BPA decomposition activities of P9@M88 in different situations. In the absence of only H_2O_2, about 5% BPA was decomposed after 60 min, which might be attributed to primary oxidation of holes or partially oxidative degradation of other active species like •OH and $•O_2^-$. With both white light and H_2O_2, P9@M88 was able to degrade 100% BPA within 30 min. The boosted BPA degradation activity of P9@M88 resulted from the enhanced formation of •OH radicals from the photo-Fenton reaction (Equations 6–8). The effect of pH and H_2O_2 addition was observed with P9@M88 as the candidate catalyst.

The effect of the initial pH value of the solution on BPA degradation is illustrated in Figure S6a. It was observed that low pH value (2.0–5.0) was beneficial to BPA degradation in this photo-Fenton reaction system, in which more than 99% degradation efficiency could be accomplished at pH 3.0 within 20 min. At pH 2.0, the degradation efficiency was lower than that at pH 3.0, as the •OH radicals were inhibited by the formation of $H_3O_2^+$ under strong acid conditions (pH < 3.0).[38] In addition, the BPA degradation rate (k value) over P9@M88 as a photo-Fenton catalyst at pH 3.0 was the highest among those at various pH values (Figure S6b). As illustrated in Figure S6c, with the increase in H_2O_2 dosage, the degradation efficiencies were gradually improved. When the dose increased to 1.2 ml/L, nearly 100% BPA was degraded within 40 min. The enhanced

removal of BPA might be attributed to the increased H_2O_2 concentration leading to more •OH generation in the photo-Fenton reaction system.

In addition, P9@M88 displayed excellent photo-Fenton decomposition activities toward the organic dyes like MB and RhB (Figure S7), in which the P9@M88 was! stable and reusable for several runs (Figures 2d, 3c and 3d).

Upon the attack of •OH radicals, the BPA molecule was degraded into some intermediates like 4-isopropenylphenol radicals (m/z = 135), hydroquinone (m/z = 109), *p*-benzoquinone (m/z = 108), phenol (m/z = 93), 4-hydroxyacetophenone (m/z = 136) and 4-isopropanolphenol (m/z = 151).[39,40] If the reaction duration was prolonged, the BPA was completely mineralized into CO_2.[41] Considering that the BPA degradation pathway with the presence of •OH radicals was well described in our previous researches,[27] the possible degradation pathway was put forward as Figure 4 based on the LC–MS determination results.

To clarify the reaction mechanism, XPS, electron spin resonance (ESR) and some electrochemical characterizations were carried out. According to the literature,[22] PANI's lowest unoccupied molecular orbital (LUMO) and highest occupied molecular orbital (HOMO) potential values are determined as −2.1 and 0.62 eV vs. NHE (normal hydrogen electrode), respectively. MIL-88A (Fe) valence states were confirmed by Mott–Schottky experiments (Figure 5a), in which the flat-band potential (E_{FB}) was approximately −0.55 eV vs. Ag/AgCl. As for the *n*-type semiconductor, the E_{FB} is 0.1 eV more positive than the conduction band potential (E_{CB}).[42] Hence, the E_{CB} of MIL-88A(Fe) was −0.45 eV vs. NHE. According to the E_g values (2.75 eV) obtained from Tauc plot of the UV–vis DRS spectrum, the valence-band potential (E_{VB}) of MIL-88A(Fe) was plotted to be 2.30 eV vs. NHE.

The XPS characterization was performed to further illuminate the charge transfer over the interface formed between MIL-88A(Fe) and PANI.[43,44] The blue shift of Fe 2p peaks from 711.68 eV in MIL-88A(Fe) to 711.52 eV in P9@M88 (Figure 5b), and the redshift of N 1 s peaks from 400.38 eV in PANI to 400.68 eV in P9@M88 (Figure 5c) could be ascribed to the additional e^- redistribution in P9@M88 system. These results corroborated the electron transfer from PANI to MIL-88A(Fe) in their P9@M88 composite, which is in good agreement with the type-II photocatalysis mechanism. As seen in Figure 5d, the electrochemical impedance spectra of the as-synthesized photocatalysts demonstrate that transfer resistance of P9@M88 is lower than those of MIL-88A (Fe) and PANI. The electrochemical impedance spectra results are in accordance with the transient photocurrent responses analyses (Figure S8), implying that the combination of PANI and MIL-88A(Fe) is a useful strategy to accelerate photogenerated e^-–h^+ pair separation to accomplish the improved photocatalysis.

The ESR spin-trap experiments of ESR spin-trap were carried out by DMPO (5,5-dimethyl-1-pyrroline N-oxide) technique to prove the main active species of the photocatalytic process. In Figures 5e and 4f, it is worth noting that $•O_2^-$ and •OH signals of P9@M88 are detected by white irradiation, but no $•O_2^-$ and •OH signals can be discovered over the individual PANI and MIL-88A (Fe) under identical conditions, respectively. Because the PANI's HOMO and MIL-88(Fe)'s valence band (VB) are not more positive than the standard potential of OH^-/•OH (2.40 eV vs NHE), the photogenerated h^+ over the surface of MIL-88A(Fe) and PANI cannot generate •OH directly. However, the •OH signals on PANI and P9@M88 generation can only be generated through a reductive mediation pathway ($O_2 \rightarrow H_2O_2 \rightarrow$ •OH). The above process is summarized in Equations 3–6.[45] As for the P9@M88/white light/H_2O_2 system, •OH is a key reactive specie in a catalytic system containing H_2O_2, which possesses strong oxidative capacity to attack most stable organic molecules.[36]

According to the above data analysis and results, the possible type-II heterojunction mechanism of the photocatalytic reaction over the P9@M88 composite was proposed (Figure 6). Both PANI and MIL-88A(Fe) could be

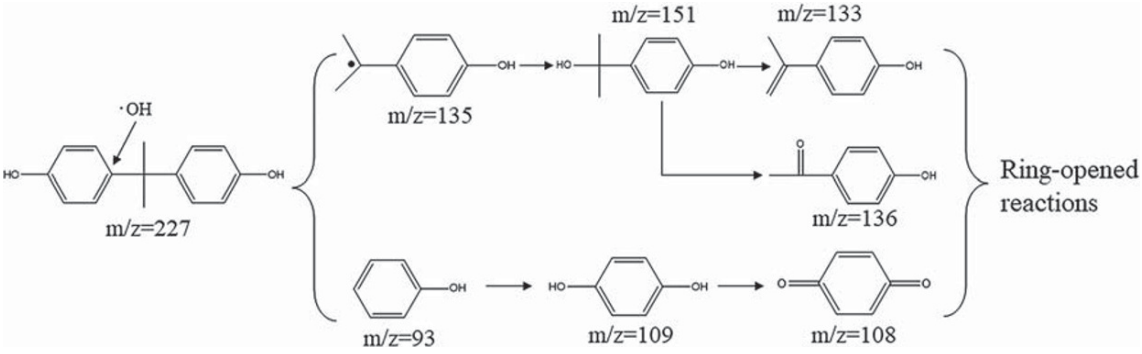

FIGURE 4 Possible photocatalytic degradation pathways of BPA degradation

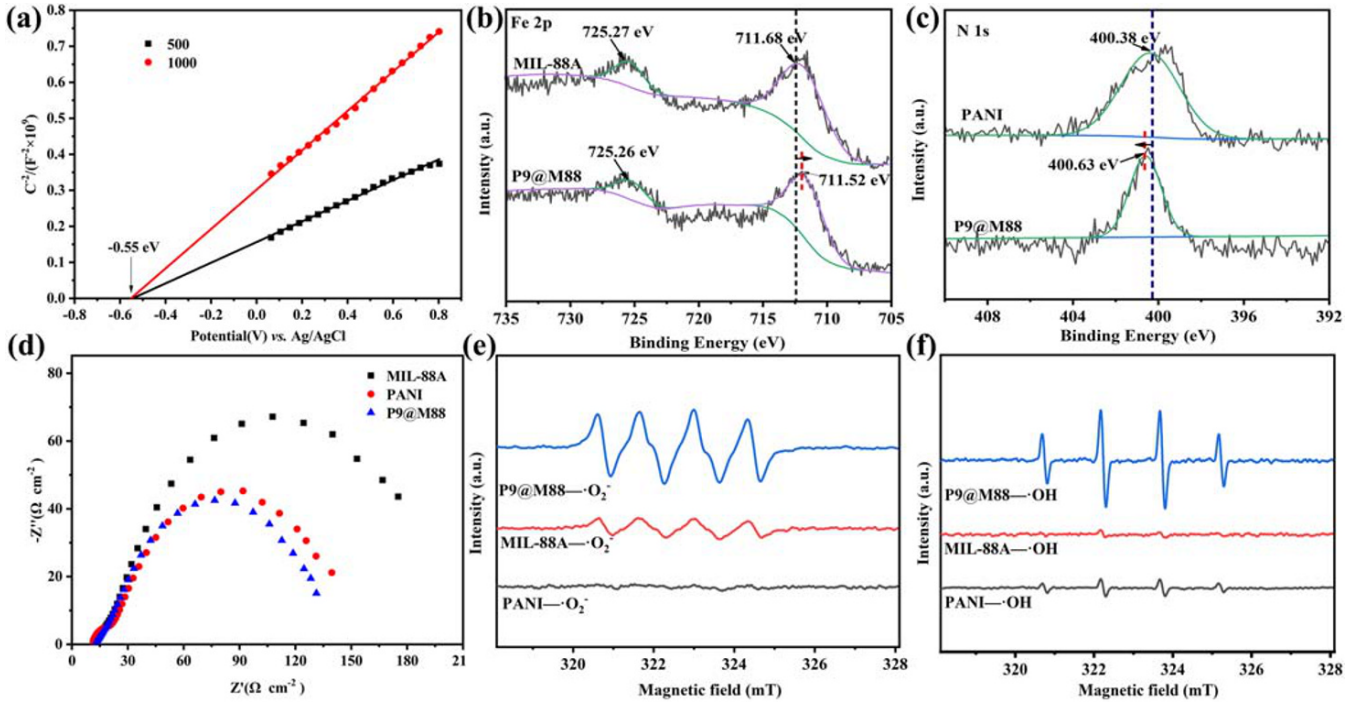

FIGURE 5 (a) Mott–Schottky plots of MIL-88A in 0.2 mol/L aqueous Na_2SO_4 solution (pH 2.0); (b, c) high-resolution XPS spectra of (b) Fe 2p for MIL-88A and P9@M88, (c) N 1 s for PANI and P9@M88. (d) Electrochemical impedance spectra plots of the samples under white light irradiation. (e, f) Electron spin resonance spectra for DMPO-•O_2^- (e) and DMPO-•OH (f) signals of the P9@M88, MIL-88A and PANI

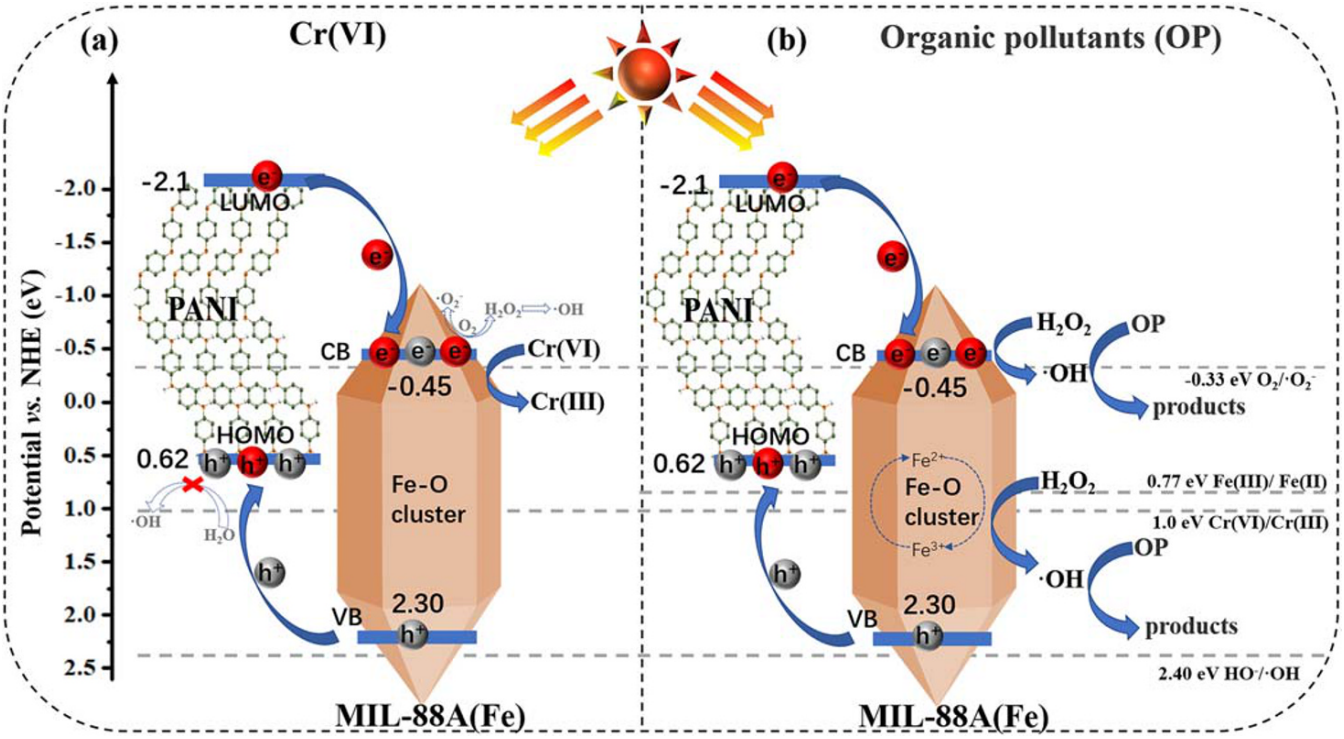

FIGURE 6 Possible photocatalytic mechanism (a) in a reduction Cr(VI) system and (b) in photo-Fenton degradation of organic pollutants system over P9@M88

stimulated by white light to produce e^- and h^+.[32,46] The photo-induced e^- can be migrated from the PANI's LUMO to the MIL-88A(Fe)'s conduction band (CB), which can accelerate the separation of photogenerated electrons–holes and lead to increasing free e^- being accumulated over the MIL-88A(Fe)'s CB. Therefore, P9@M88 exhibited enhanced Cr(VI) reduction efficiency under white light irradiation. The MIL-88A(Fe)'s CB was more negative than the $O_2/\bullet O_2^-$ standard redox potential (−0.33 eV vs. NHE). Then, the accumulated e^- in MIL-88A(Fe)'s CB reacted directly with O_2 to generate $\bullet O_2^-$, and to produce •OH indirectly,[47] which were responsible for the decomposition of organic pollutants. The CB position (−0.45 eV vs. NHE) of MIL-88A(Fe) was more negative than the Fe^{3+}/Fe^{2+} standard potential of (0.77 eV vs. NHE).[37] The partial electrons over MIL-88A (Fe) that were photo-excited by white light could both participate in the Fe^{3+}/Fe^{2+} circulation process and activate H_2O_2 to produce •OH radicals (Equations 7–8). The •OH radicals yielded by the photo-Fenton reaction contributed to the elimination of organic pollutants like BPA, MB and RhB.[48] In addition, H_2O_2 as an efficient electronic scavenger could capture the photogenerated e^- in the excited P9@M88 to generate •OH radicals (Equation 6).[36,48] PANI's HOMO (0.62 eV vs. NHE) cannot attain the $OH^-/\bullet OH$ potential (2.40 eV vs. NHE), so the aggregated h^+ in the PANI's HOMO could oxidize directly the organic pollutants rather than oxidizing H_2O to form •OH.

$$\text{P9@M88} + h\nu \rightarrow \text{P9@M88}\,(h^+ + e^-) \quad (3)$$

$$O_2 + e^- \rightarrow \bullet O_2^- \quad (4)$$

$$O_2 + 2H^+ + 2e^- \rightarrow H_2O_2 \quad (5)$$

$$H_2O_2 + e^- \rightarrow \bullet OH + HO^- \quad (6)$$

$$Fe\,(III) + H_2O_2 \rightarrow Fe\,(II) + \bullet HOO + H^+ \quad (7)$$

$$Fe\,(II) + H_2O_2 \rightarrow Fe\,(III) + \bullet OH + OH^- \quad (8)$$

4 | CONCLUSIONS

In all, PANI/MIL-88A(Fe) (Px@M88) composites were fabricated by a simple one-pot hydrothermal reaction process. The introduction of PANI can improve the conductivity of MIL-88A(Fe), accelerate separation of photo-induced charge carriers and enhance the utilization of visible light. The photocatalytic Cr(VI) reduction efficiency of P9@M88 was 3.5-fold higher than that of individualized MIL-88A(Fe). When H_2O_2 was added, the photo-Fenton reaction was excited over P9@M88 composite to achieve the efficient degradation of organic pollutants like BPA, MB and RhB, which can be assigned to the boosted production of hydroxyl radicals in the photo-Fenton reaction. The BPA degradation pathway and the photocatalysis mechanism over P9@M88 were proposed and verified. Last but not least, P9@M88 composite can be recycled and reused to achieve efficient removal of both Cr(VI) and three organic pollutants. Further investigations will be conducted to tap more efficient MOF composites for application in water environment restoration.

ACKNOWLEDGMENTS

This work was financially supported by by National Natural Science Foundation of China (nos 51878023, 51578034), Great Wall Scholars Training Program Project! of Beijing Municipality Universities (CIT and TCD20180323), Beijing Talent Project (2019A22) and BUCEA Post Graduate Innovation Project (PG2019041).

ORCID

Chong-Chen Wang https://orcid.org/0000-0001-6033-7076

REFERENCES

[1] F. Martínez, R. Sanz, G. Orcajo, D. Briones, V. Yángüez, *Chem. Eng. Sci.* **2016**, *142*, 55.
[2] Y. Zhao, H. Ding, Q. Zhong, *Appl. Surf. Sci.* **2013**, *284*, 138.
[3] A. Crake, K. C. Christoforidis, A. Kafizas, S. Zafeiratos, C. Petit, *Appl. Catal. Environ.* **2017**, *210*, 131.
[4] Y. Su, Z. Zhang, H. Liu, Y. Wang, *Appl. Catal. Environ.* **2017**, *200*, 448.
[5] X. Shi, J. Zhang, G. Cui, N. Deng, W. Wang, Q. Wang, B. Tang, *Nano Res.* **2018**, *11*, 979.
[6] Y. Gao, S. Li, Y. Li, L. Yao, H. Zhang, *Appl. Catal. Environ.* **2017**, *202*, 165.
[7] C. Yang, X. You, J. Cheng, H. Zheng, Y. Chen, *Appl. Catal. Environ.* **2017**, *200*, 673.
[8] W. Huang, C. Jing, X. Zhang, M. Tang, L. Tang, M. Wu, N. Liu, *Chem. Eng. J.* **2018**, *349*, 603.
[9] X.-D. Du, X.-H. Yi, P. Wang, W. Zheng, J. Deng, C.-C. Wang, *Chem. Eng. J.* **2019**, *356*, 393.
[10] F.-X. Wang, X.-H. Yi, C.-C. Wang, J.-G. Deng, *Chinese J. Catal.* **2017**, *38*, 2141.
[11] Z. Yang, J. Cao, Y. Chen, X. Li, W. Xiong, Y. Zhou, C. Zhou, R. Xu, Y. Zhang, *Microporous Mesoporous Mater.* **2019**, *277*, 277.
[12] H. Wang, X. Yuan, Y. Wu, G. Zeng, X. Chen, L. Leng, Z. Wu, L. Jiang, H. Li, *J. Hazard. Mater.* **2015**, *286*, 187.
[13] R. Liang, F. Jing, L. Shen, N. Qin, L. Wu, *J. Hazard. Mater.* **2015**, *287*, 364.

[14] X. Zhang, L. Song, F. Bi, D. Zhang, Y. Wang, L. Cui, *J. Colloid Interface Sci.* **2020**, *571*, 38.
[15] C.-C. Wang, X.-H. Yi, P. Wang, *Appl. Catal. Environ.* **2019**, *247*, 24.
[16] C.-C. Wang, X.-D. Du, J. Li, X.-X. Guo, P. Wang, J. Zhang, *Appl. Catal. Environ.* **2016**, *193*, 198.
[17] C.-C. Wang, X. Wang, W. Liu, *Chem. Eng. J.* **2019**, 123601.
[18] J. Chen, X. Zhang, F. Bi, X. Zhang, Y. Yang, Y. Wang, *J. Colloid Interface Sci.* **2020**, *571*, 275.
[19] F. Bi, X. Zhang, J. Chen, Y. Yang, Y. Wang, *Appl. Catal. Environ.* **2020**, *269*, 118767.
[20] X. Xu, R. Liu, Y. Cui, X. Liang, C. Lei, S. Meng, Y. Ma, Z. Lei, Z. Yang, *Appl. Catal. Environ.* **2017**, *210*, 484.
[21] L. He, Y. Dong, Y. Zheng, Q. Jia, S. Shan, Y. Zhang, *J. Hazard. Mater.* **2019**, *361*, 85.
[22] D.-D. Chen, X.-H. Yi, C. Zhao, H. Fu, P. Wang, C.-C. Wang, *Chemosphere* **2020**, *245*, 125659.
[23] H. Fida, S. Guo, G. Zhang, *J. Colloid Interface Sci.* **2015**, *442*, 30.
[24] X. Li, H. Liu, X. Jia, G. Li, T. An, Y. Gao, *Sci. Total Environ.* **2018**, *621*, 1533.
[25] J. Li, C. Xiao, K. Wang, Y. Li, G. Zhang, *Environ. Sci. Technol.* **2019**, *53*, 11023.
[26] Y. Yan, H. Yang, Z. Yi, T. Xian, R. Li, X.-x. Wang, *Desalin. Water Treat.* **2019**, 349.
[27] H. Fu, X.-X. Song, L. Wu, C. Zhao, P. Wang, C.-C. Wang, *Mater. Res. Bull.* **2020**, *125*, 110806.
[28] Y. Lin, D. Li, J. Hu, G. Xiao, J. Wang, W. Li, X. Fu, *J. Phys. Chem. C* **2012**, *116*, 5764.
[29] W. Wu, J. Wang, T. Zhang, S. Jiang, X. Ma, G. Zhang, X. Zhang, X. Chen, B. Li, *J. Mater. Chem. C* **2019**, *7*, 5451.
[30] M. Nandi, R. Gangopadhyay, A. Bhaumik, *Microporous Mesoporous Mater.* **2008**, *109*, 239.
[31] J. Zhang, Y. Hu, X. Jiang, S. Chen, S. Meng, X. Fu, *J. Hazard. Mater.* **2014**, *280*, 713.
[32] Z. Shao, D. Zhang, H. Li, C. Su, X. Pu, Y. Geng, *Sep. Purif. Technol.* **2019**, *220*, 16.
[33] L. Shi, T. Wang, H. Zhang, K. Chang, X. Meng, H. Liu, J. Ye, *Adv. Sci.* **2015**, *2*, 1500006.
[34] C. Wang, L. Zhu, M. Wei, P. Chen, G. Shan, *Water Res.* **2012**, *46*, 845.
[35] C. Zhao, Z. Wang, X. Li, X. Yi, H. Chu, X. Chen, C.-C. Wang, *Chem. Eng. J.* **2019**, 123431.
[36] M. Cheng, C. Lai, Y. Liu, G. Zeng, D. Huang, C. Zhang, L. Qin, L. Hu, C. Zhou, W. Xiong, *Coord. Chem. Rev.* **2018**, *368*, 80.
[37] T. Guo, K. Wang, G. Zhang, X. Wu, *Appl. Surf. Sci.* **2019**, *469*, 331.
[38] Q. Chen, P. Wu, Y. Li, N. Zhu, Z. Dang, *J. Hazard. Mater.* **2009**, *168*, 901.
[39] J. Du, J. Bao, Y. Liu, H. Ling, H. Zheng, S. H. Kim, D. D. Dionysiou, *J. Hazard. Mater.* **2016**, *320*, 150.
[40] J. Zhang, X. Zhao, Y. Wang, Y. Gong, D. Cao, M. Qiao, *Appl. Catal. Environ.* **2018**, *237*, 976.
[41] N. Lu, Y. Lu, F. Liu, K. Zhao, X. Yuan, Y. Zhao, Y. Li, H. Qin, J. Zhu, *Chemosphere* **2013**, *91*, 1266.
[42] C.-W. Zhao, Y.-A. Li, X.-R. Wang, G.-J. Chen, Q.-K. Liu, J.-P. Ma, Y.-B. Dong, *Chem. Commun.* **2015**, *51*, 15906.
[43] J. Low, B. Dai, T. Tong, C. Jiang, J. Yu, *Adv. Mater.* **2019**, *31*, 1802981.
[44] Q. Xu, B. Zhu, C. Jiang, B. Cheng, J. Yu, *Solar RRL* **2018**, *2*, 1800006.
[45] J. Sheng, X. Li, Y. Xu, *ACS Catal.* **2014**, *4*, 732.
[46] L. Liu, L. Ding, Y. Liu, W. An, S. Lin, Y. Liang, W. Cui, *Appl. Catal. Environ.* **2017**, *201*, 92.
[47] J. Lim, H. Kim, J. Park, G.-H. Moon, J. J. M. Vequizo, A. Yamakata, J. Lee, W. Choi, *Environ. Sci. Technol.* **2020**, *54*, 497.
[48] L. Ai, C. Zhang, L. Li, J. Jiang, *Appl. Catal. Environ.* **2014**, *148-149*, 191.

SUPPORTING INFORMATION

Additional supporting information may be found online in the Supporting Information section at the end of this article.

How to cite this article: Chen D-D, Yi X-H, Ling L, Wang C-C, Wang P. Photocatalytic Cr(VI) sequestration and photo-Fenton bisphenol A decomposition over white light responsive PANI/MIL-88A(Fe). *Appl Organomet Chem*. 2020;e5795. https://doi.org/10.1002/aoc.5795